

XPS, XANES and EXAFS investigations of CuO/ZnO/Al₂O₃/ZrO₂ mixed oxide catalysts

S. Velu,^{†a} K. Suzuki,^a Chinnakonda S. Gopinath,^b H. Yoshida^c and T. Hattori^c

^a Ceramics Research Institute, National Institute of Advanced Industrial Science and Technology, Nagoya, 463-8560, Japan. E-mail: subravelu@hotmail.com

^b Catalysis Division, National Chemical Laboratory, Pune, 411 008, India. E-mail: gopi@cata.ncl.res.in

^c Department of Applied Chemistry, Graduate School of Engineering, Nagoya University, Nagoya, 464-8603, Japan. E-mail: yoshidah@apchem.nagoya-u.ac.jp

Received 25th October 2001, Accepted 5th February 2002

First published as an Advance Article on the web 18th April 2002

Systematic X-ray photoelectron spectroscopy (XPS), X-ray induced Auger electron spectroscopy (AES), X-ray absorption near edge structure (XANES) and extended X-ray absorption fine structure (EXAFS) studies were undertaken to investigate the electronic structure, chemical states and local geometry of the active species in the CuO/ZnO/Al₂O₃/ZrO₂ multicomponent mixed oxide catalysts employed in the oxidative steam reforming of methanol (OSRM) reaction for H₂ production. The core level XPS and AES indicated the existence of CuO and ZnO-like species. Two kinds of zirconium species, one similar to that of ZrO₂ and another with relatively higher electron density were noticed from the Zr 3d core level XPS of Zr-containing catalysts. The valence band (VB) XPS studies revealed that for Zr-containing catalysts, the Cu 3d anti-bonding orbital splits from the main VB and shifts toward lower binding energy (BE). The surface Cu/(Al + Zr) ratios were found to be close to those in the bulk while segregation of Zn at the surface was evidenced in all samples. The XANES and EXAFS results also indicated the existence of CuO and ZnO-like species, whose local environments are modified with respect to the chemical composition. The EXAFS study of the Zr-containing catalysts indicated the existence of a “Cu–O–Zr” bonding with a Cu–Zr distance in the range 3.5 to 3.9 Å. The results indicated the existence of a Cu–Zr synergistic interaction in these catalysts which improved the catalytic performance in the OSRM reaction.

1 Introduction

CuO/ZnO/Al₂O₃ and CuO/ZnO/ZrO₂ mixed oxide catalysts are very active and selective in various industrially important chemical processes including CO/CO₂ hydrogenation for methanol synthesis, CO oxidation, the water–gas shift reaction, *etc.*^{1–7} A potential new application of these CuO/ZnO-based mixed oxide catalysts in recent years is their use in methanol reforming to produce H₂ for fuel cells, because on-board generation of H₂ from methanol coupled with a proton-exchange membrane fuel cell (PEMFC) is considered to be one of the attractive options for low-emission passenger automobiles in the future. Thus, the steam reforming of methanol (SRM) and partial oxidation of methanol (POM) reactions over CuO/ZnO/Al₂O₃ and CuO/ZnO/Al₂O₃/ZrO₂ mixed oxide catalysts have been reported.^{8–10} Very recently, it has been demonstrated^{11–14} that a combined steam reforming and partial oxidation reaction, which has been called “oxidative steam reforming of methanol” OSRM over CuO/ZnO/Al₂O₃/ZrO₂ mixed oxide catalysts is the most convenient method for on-board H₂ generation for fuel cells.

The chemical composition of the CuO/ZnO/Al₂O₃/ZrO₂ mixed oxide catalysts exhibited a significant influence on their performance in the OSRM reaction. A decrease in Al content

as well as an increase in Zr content improved the catalytic activity towards methanol conversion and the H₂ production rate. Earlier studies¹² revealed that a part of the copper (referred to as isolated Cu²⁺ species) in Al-rich samples interacts with Al due to the formation of amorphous CuAl₂O₄ spinel at the surface, and this is reduced at relatively higher temperatures than the Al-free analogue. Furthermore, the copper metal surface area and dispersion were enhanced with decreasing Al content. Breen and Ross,⁹ based on the temperature programmed reduction (TPR) of Cu/ZnO/ZrO₂ catalysts, have concluded the occurrence of a redox mechanism at the boundary layers of metallic copper in intimate contact with ZnO. Suh *et al.*,⁷ with their methanol synthesis Cu/ZnO/ZrO₂ catalysts, have concluded that a part of the zirconium ions is dissolved in the copper oxide lattice. Copper and zirconia in these catalyst systems are reported to behave in a bifunctional manner.¹⁵

XPS, XANES and EXAFS measurements have been employed for the characterization of CuO/ZnO binary and, in a few cases, CuO/ZnO/Al₂O₃ ternary oxides.^{1,4,10,16–18} Unfortunately, to the best of our knowledge no systematic XPS and XAS study has been reported in the literature on CuO/ZnO/ZrO₂ or CuO/ZnO/Al₂O₃/ZrO₂ multicomponent mixed oxide catalysts, which are more active and selective in methanol synthesis, SRM and OSRM reactions.

The aim of the present investigation was to explore the electronic structure, in particular the chemical state and the local geometry of active species in the CuO/ZnO/Al₂O₃/ZrO₂ mul-

[†] Present address: Department of Energy and Geo-Environmental Engineering, Energy Institute, Pennsylvania State University, University Park, PA 16802, USA. E-mail: vx23@psu.edu

ticomponent mixed oxide catalysts using combined XPS, XANES and EXAFS spectroscopies. The catalytic performance of the CuO/ZnO/Al₂O₃/ZrO₂ mixed oxide catalysts of the present study has already been employed in the OSRM reaction to produce H₂ for fuel cell applications.^{11–14} Hence, a detailed spectroscopic study will be useful to understand the nature of the interaction between copper and zirconia, not only for the CuO/ZnO/ZrO₂ mixed oxide catalysts employed in the OSRM reaction but also in those developed recently for the SRM, methanol synthesis and methanol decomposition reactions.^{5,7–9,15}

2 Experimental

2.1 Catalyst preparation and bulk characterization

The CuO/ZnO-based mixed oxide catalysts were prepared by the thermal decomposition, at 450 °C, of CuZn-based hydroxalcalite (HT)-like layered double hydroxides (LDHs) precursors. The LDH precursors were synthesized by coprecipitation of an aqueous solution of mixed metal nitrates with a mixer of NaOH and Na₂CO₃ at a constant pH (≈10). Detailed procedures for the catalyst preparation and characterization using X-ray fluorescence spectroscopy (XRF), X-ray diffraction (XRD), ultraviolet diffuse reflectance spectroscopy (DRS), temperature programmed reduction (TPR) and EPR techniques and the measurement of copper metal surface areas by N₂O passivation and CO chemisorption have been described elsewhere.^{12,14}

2.2 XPS measurements

The core level XP spectra and the X-ray induced Auger electron (AE) spectra were acquired from a VG Microtech MultiLab ESCA 3000 spectrometer. All measurements were made at room temperature using a non-monochromatized Mg-Kα X-ray source ($h\nu = 1253.6$ eV) on powder samples. The base pressure in the analysis chamber was maintained in the $3\text{--}6 \times 10^{-10}$ Torr range. The energy resolution of the spectrometer was set at 0.8 eV with Mg-Kα radiation at a pass energy of 20 eV. The BE was calibrated with respect to Au 4f_{7/2} core level at 83.9 eV. The BE of adventitious carbon (284.9 eV) was used for charge correction. The error in all the BE values reported in the present study is within 0.1 eV.

2.3 XANES and EXAFS measurements

The XAFS spectra were recorded on a commercial XAFS spectrometer (Laboratory EXAFS, EXAC 820, Technos Co. Ltd).¹⁹ The X-ray source is a rotating anode X-ray generator operating at 17 kV, 150 mA; the low voltage was employed to avoid contamination by high energy X-rays from higher

order reflections. The target anode was Mo, and LaB₆ was used as the filament material. A single monochromator was employed using a Johansson-type Ge(220) bent crystal curved with Rowland circle geometry ($R = 300$ mm). The second order reflection was used for measurements. The spectra were recorded in transmission mode at room temperature and in ambient atmosphere. The X-ray intensity before passing the sample, I_0 , was detected with a semi-transmitting sealed proportional counter (S-PC) filled with 0.5 atm of Ar and the intensity after passing the sample, I , was detected with a pure-Ge solid state detector (SSD). Data processing was performed using a computer program supplied with the EXAC 820 instrument. XANES spectra were normalized to the height of the edge jump after subtracting the contribution from absorption other than the K-edge absorption by the Cu or Zn atoms. Energy calibration was carried out using the characteristic Cu K-edge peak at 8978.9 eV of Cu foil.^{20,21} Curve fitting analysis on Fourier-filtered EXAFS in k-space was carried out using theoretical phase shifts and amplitudes for Cu–O, Cu–Cu and Cu–Zr atom pairs taken from FEFF6.²² There were three free parameters for fitting: N , the coordination number; R , the distance and σ^2 the Debye–Waller factor for each shell.

3 Results

3.1 Bulk characterization (XRD and chemical analyses)

The physicochemical properties such as chemical composition and XRD phases of the CuO/ZnO/Al₂O₃/ZrO₂ mixed oxide catalysts have already been reported.¹² For a better understanding of the nature of the materials, the results are summarized in Table 1 and briefly described below. For all samples, the copper content was kept constant while varying the Zn, Al and Zr contents. Al was partially substituted by Zr in the sample CZAZOC-6, while in CZAZOC-7 it was completely replaced by Zr (see Table 1). The XRD of the uncalcined samples exhibited hydroxy carbonates containing hydroxalcalite (HT)-like layered double hydroxide (LDH; JCPDS file No. 38-487) as a primary phase.¹³ As the Al content decreased, other phases such as aurichalcite, [(Cu,Zn)₅(CO₃)₂(OH)₆; JCPDS file No.7-743] and bayerite [Al(OH)₃; JCPDS file No.20-11] were also noticed besides the LDH phase. The specimen CZAZOC-7, without Al, exhibited an exclusive aurichalcite phase. Thermal decomposition of these CuZnAl(Zr) hydroxycarbonate precursors at 450 °C for 5 h generated a mixture of CuO and ZnO phases. The crystallinity of the resulting materials was very poor for Al-rich CZAZOC-1 but increased gradually with decreasing Al content. The XRD lines corresponding to ZnO were dominant compared to those of CuO in all samples. The OSRM reaction was performed over these calcined samples after reducing them *in situ* in flowing H₂

Table 1 Chemical compositions and XRD phases of CuO/ZnO/Al₂O₃/ZrO₂ mixed catalysts

Catalyst	Metal composition (wt.%) ^a				Cu/(Al + Zr) atomic ratio ^a	XRD phases		
	Cu	Zn	Al	Zr		Uncalcined ^b	Calcined	D^c / Å
CZAZOC-1	35.3	44.1	20.6	0.0	0.74	LDH	ZnO ^d + CuO ^d	ND
CZAZOC-4	37.6	50.7	11.7	0.0	1.37	LDH + AH + AC	ZnO + CuO	ND
CZAZOC-5	37.9	53.0	9.1	0.0	1.76	LDH + AH + AC	ZnO + CuO	ND
CZAZOC-6	35.9	44.7	5.1	14.3	1.68	AC + LDH + AH	ZnO + CuO	107
CZAZOC-7	32.3	40.5	0.0	27.2	1.70	AC	ZnO ^e + CuO ^e	85

^a Chemical analysis result obtained from XRF spectroscopy. ^b LDH: Layered double hydroxide [(Cu,Zn)₆Al₂(OH)₁₆CO₃·4H₂O], JCPDS file 38-487; AH: Al(OH)₃ (bayerite), JCPDS file 20-11; AC: Aurichalcite [(Zn,Cu)₅(CO₃)₂(OH)₆], JCPDS file 7-743. ^c D , Crystallite size of CuO particles calculated from the (200) plane using the Scherrer equation. ND: Crystallite sizes are not determined because of the overlapping of CuO peaks with ZnO in those samples. ^d Poorly crystallized and the crystallinity gradually increases from CZAZOC-1 to CZAZOC-7. ^e Well crystallized.

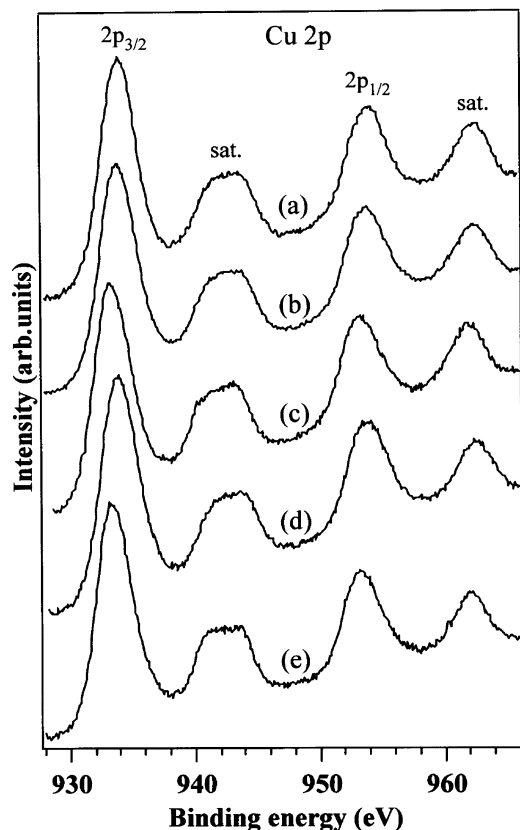


Fig. 1 Cu 2p core level X-ray photoelectron spectra of CuO/ZnO/Al₂O₃/ZrO₂ mixed oxide catalysts. (a) CZAZOC-1, (b) CZAZOC-4, (c) CZAZOC-5, (d) CZAZOC-6, (e) CZAZOC-7.

at 300 °C for 3 h. It was found from *in situ* XRD measurements (unpublished results) that the CuO phase was reduced to metallic copper upon H₂ reduction. However, all the samples characterized in the present study were in the calcined form without H₂-reduction.

3.2 XPS and AES

Fig. 1 depicts the Cu 2p core level XP spectra for a series of CuO/ZnO/Al₂O₃/ZrO₂ mixed oxide catalysts. The XPS parameters are summarized in Table 2. It can be seen that these samples exhibit Cu 2p_{3/2} and Cu 2p_{1/2} main peaks in the BE ranges 933 to 934 eV and 953 to 954 eV, respectively with a spin-orbit coupling energy gap 20 eV. Based on the BE values (933.9 ± 0.1 eV), the samples CZAZOC-1, CZAZOC-4 and CZAZOC-6 can be grouped as set 1 and those CZAZOC-5 and CZAZOC-7 with a BE of 933.3 eV as set 2. It can also

be noticed that both Cu 2p_{3/2} and Cu 2p_{1/2} peaks are accompanied by intense satellite features at 942 and 962 eV for all samples. The intensity ratio between the satellite and the Cu 2p_{3/2} main band ($I_S/I_M = 0.40$ to 0.46) and the full-width at half maximum (FWHM = 3.4 ± 0.1 eV) are almost the same for all the catalysts.

The X-ray induced AES of these samples are presented in Fig. 2 in the kinetic energy (KE) region between 904 and 930 eV. The XPS spectrum of pure ZrO₂ reference sample in the Zr 3p region is also included in the same figure. The position of the peaks due to the Cu L₃M₄₅M₄₅ (hereafter referred to as Cu LMM) transition of Cu²⁺ in the KE range 913–919 eV can be clearly distinguished from Zr 3p_{5/2} at 920.8 eV in the Zr-containing samples and the data are included in Table 2. As observed in the core level, the position of the Cu Auger peak also shifts with respect to the chemical composition. The modified Auger parameter (α') has been used to determine the chemical state of copper in these samples. The parameter α' is defined as;¹

$$\alpha' = E_B + E_K \quad (1)$$

where, E_B is the binding energy of the Cu 2p_{3/2} core level and E_K is the kinetic energy of the Cu LMM Auger electron. The α' values determined using eqn. (1) are included in Table 2 together with the data of some of the reference samples containing Cu²⁺ reported in the literature.^{1,2,3,24} As observed in the Cu 2p core level, samples can be grouped into two sets based on their similar Cu LMM KE and α' parameters. The set 1 samples comprising CZAZOC-1, CZAZOC-4 and CZAZOC-6 have Cu L₃M₄₅M₄₅ and α' values 916.8 ± 0.2 eV and 1850.8 ± 0.1 eV, respectively while these parameters for set 2 samples, which include CZAZOC-5 and CZAZOC-7, are 918.1 ± 0.1 eV and 1851.5 ± 0.1 eV, respectively. The difference in the above set of values clearly points to a different electron density on the copper atoms.

In an attempt to understand the difference in the chemical states of the copper species present in set 1 and set 2 catalyst, the Wagner plot, as reported earlier,²⁵ has been drawn and is shown in Fig. 3. Here, the kinetic energy of the Auger transition on the Y axis and the Cu 2p_{3/2} binding energy of the photoemission line on the X-axis, in the negative direction for all the catalysts are plotted. The data for Cu, Cu₂O and CuO reference samples reported in the literature^{1,2,6} are also plotted in the same figure. The Auger parameters are described by solid straight lines with a slope of -1. Compounds with similar initial state effects are described in the Wagner plot by a straight line with a slope of -3.²⁵ A slope of (-2.3) close to the -3 for the present catalyst systems would indicate that the initial states are similar, although they are of less importance. However, the higher Auger parameters of set 2 catalysts indicate the contribution of higher values of extra-atomic relaxation energy and hence a different final state compared

Table 2 XPS and AES parameters of Cu 2p_{3/2} from CuO/ZnO/Al₂O₃/ZrO₂ mixed catalysts

Catalyst	BE of Cu 2p _{3/2} /eV	FWHM /eV	I_S/I_M	KE of Cu L ₃ M ₄₅ M ₄₅ /eV	α' /eV
CZAZOC-1	934.0	3.2	0.45	916.7	1850.7
CZAZOC-4	933.8	3.3	0.46	916.9	1850.7
CZAZOC-5	933.3	3.3	0.41	918.2	1851.5
CZAZOC-6	933.9	3.3	0.40	917.0	1850.9
CZAZOC-7	933.4	3.1	0.44	918.0	1851.4
CuZnAl-HT ^a	934.6	3.8	—	916.0	1850.6
Malachite ^a	934.6	3.3	—	916.8	1851.4
CuO ^b	933.8	3.6	0.55	917.6	1851.4
CuAl ₂ O ₄ ^c	935.0	—	—	916.5	1851.5

^a Ref. 23. ^b Ref. 1. ^c Ref. 24.

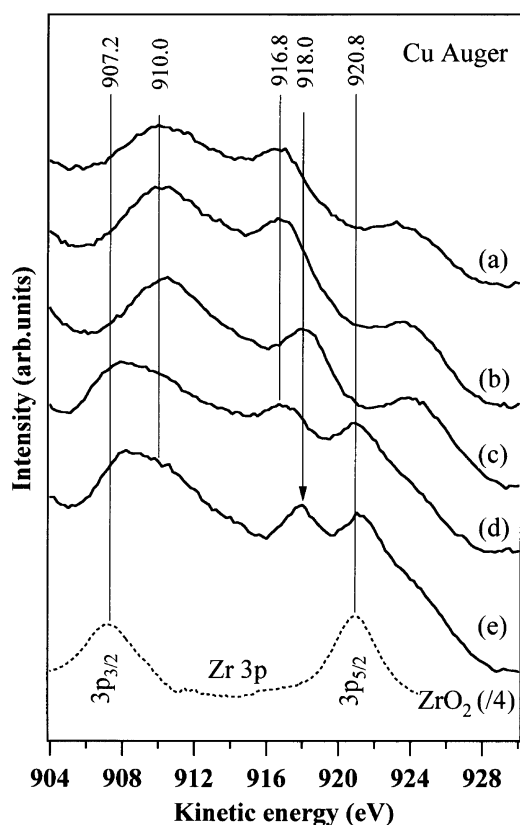


Fig. 2 X-ray induced Auger electron spectra of CuO/ZnO/Al₂O₃/ZrO₂ mixed oxide catalysts. (a) CZAZOC-1, (b) CZAZOC-4, (c) CZAZOC-5, (d) CZAZOC-6, (e) CZAZOC-7. The core level XPS spectrum of ZrO₂ in the 3p region is also included.

to set 1 catalysts. It can be seen from the Wagner plot that set 2 catalysts and CuO fall on the same line, in spite of the electron-rich environment of the catalysts. The photoemission results of set 2 catalysts are in proximity to both CuO and metallic copper, and this accounts for its crystalline CuO character, as evidenced from the XRD, and electron-rich environment, respectively. The set 1 catalysts fall on the line of metallic copper but exhibit low Auger parameters. This could be due to the

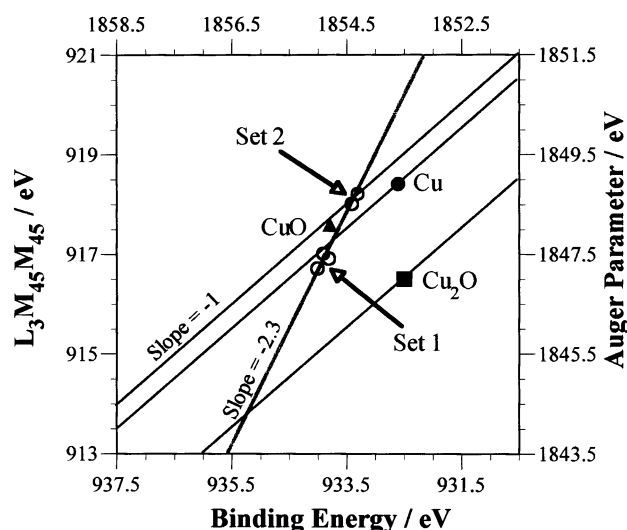


Fig. 3 Wagner plot for CuO/ZnO/Al₂O₃/ZrO₂ mixed oxide catalysts and Cu-containing reference samples. Solid lines and dotted lines are with a slope of -1 and -2.3 for Cu-containing reference samples and CuO/ZnO/Al₂O₃/ZrO₂ mixed oxide catalysts, respectively.

poor crystallinity of the CuO phase, as observed from the XRD, and the higher ionicity of the chemical bond²⁵ in this set of catalysts (set 1 catalysts). Nevertheless, the results are complex and further experimental evidence is required.

Zn 2p_{3/2} core level XP spectra of all the samples (not shown) exhibited an intense peak at 1021.9 ± 0.2 eV with a FWHM value about 2.2 ± 0.1 eV, very close to the BE ($1021.3 - 1022.0$ eV) and FWHM (2.0 eV) of the ZnO reference.²³ This revealed that the chemical environment of Zn was not influenced significantly by the chemical composition.

Zr 3d core level XP spectra of CZAZOC-6 containing both Al and Zr and CZAZOC-7 without Al are shown in Fig. 4 together with the spectrum of pure ZrO₂. It can be seen that the pure ZrO₂ exhibits a spin-orbit doublet of the 3d core level into 3d_{5/2} (182.1 eV) and 3d_{3/2} (184.5 eV) levels with an energy gap 2.4 eV between them and a relative intensity ratio ($I_{3d_{5/2}}/I_{3d_{3/2}}$) of 1.6. These values are in excellent agreement with those reported in the literature for pure ZrO₂.²⁷ The samples, CZAZOC-6 and CZAZOC-7 also exhibit a similar doublet in the same BE region, indicating the existence of ZrO₂-like species. However, compared to ZrO₂, the catalysts exhibit a broad band and also the intensity of the valley between the spin-orbit doublets is less. Deconvolution of the original spectra produces peaks attributed to the existence of at least two kinds of Zr⁴⁺ species, namely species I at low BE and species II at high BE, which differ in their chemical environments. A spin-orbit energy gap of 2.4 eV and an intensity ratio close to 60:40 for 3d_{5/2}:3d_{3/2} have been imposed in the above deconvolution. The peak positions and their contributions extracted from the deconvolution are summarized in Table 3. The intensity of the valley between the spin-orbit doublets is less deep in the case of CZAZOC-6, indicating a larger contribution of higher BE Zr species (species II). The concentration of species I increases at the expense of species II in CZAZOC-7. It can be

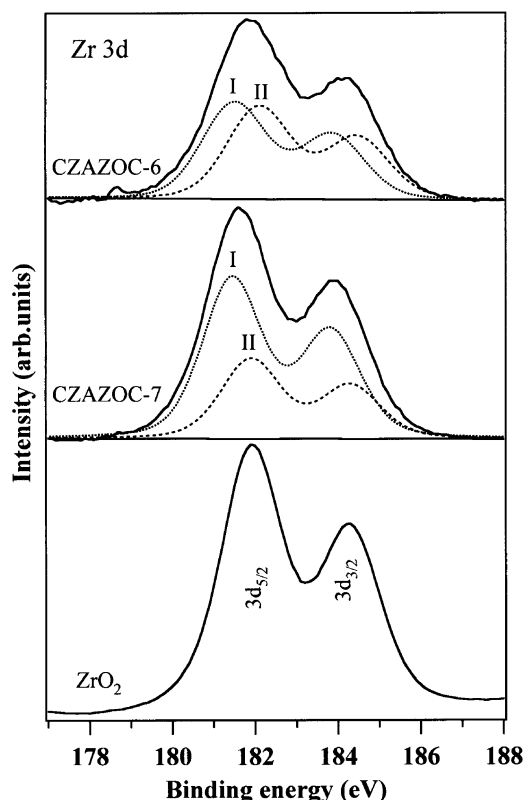


Fig. 4 Zr 3d core level X-ray photoelectron spectra of CZAZOC-6 and CZAZOC-7 catalysts. Zr 3d core levels are deconvoluted to show the presence of two species. Species I occurs at low BE and species II at high BE. The spectrum of pure ZrO₂ is presented for comparison.

Table 3 XPS parameters of Zr 3d core level on CuO/ZnO/Al₂O₃/ZrO₂ mixed oxide catalysts and pure ZrO₂ reference sample

Catalyst	BE of Zr 3d _{3/2} core level /eV	
	Species I (Intensity(%))	Species II (Intensity(%))
CZAZOC-6	181.5 (51.1)	182.1 (48.9)
CZAZOC-7	181.4 (66.8)	181.9 (33.2)
ZrO ₂	None	181.9 (100)

noticed that the BE of species II is very close to that of ZrO₂ and hence they are assigned to ZrO₂-like species. The observation of an additional lower BE Zr species (species I) in these catalysts is interesting and suggests the formation, at the surface, of zirconium sites having relatively higher electron density. The presence of a similar lower BE Zr⁴⁺ species has been observed in Fe(NO₃)₃ impregnated ZrO₂ and this indicated the involvement of redox mechanism in the iron-promoted zirconia catalysts.²⁷

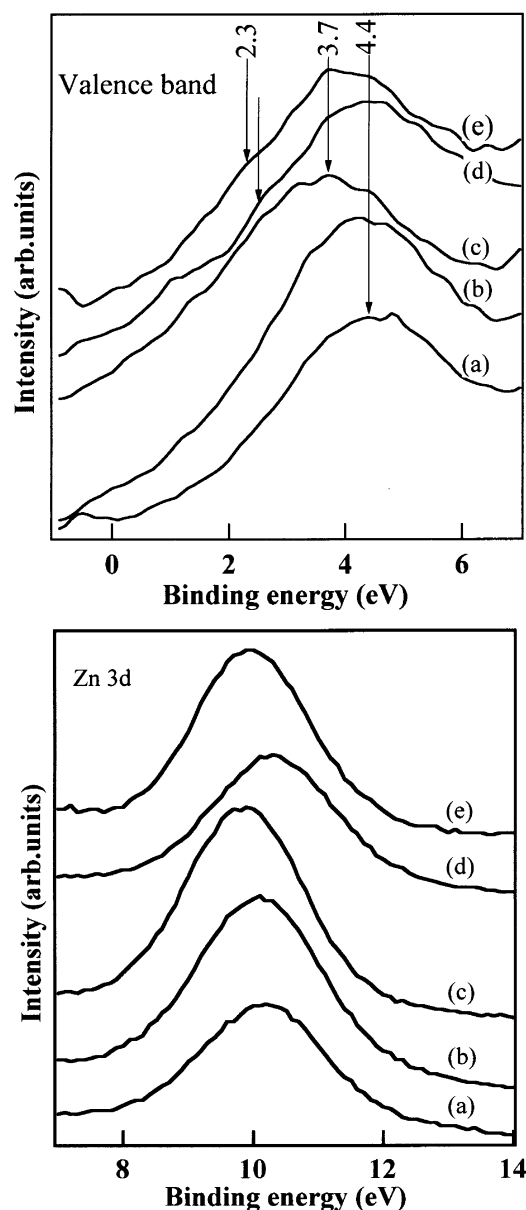
Valence bands are those occupied by electrons of low BE (below 15 eV), which are essentially involved in the bonding orbitals. The measurement of spectra in this region is very useful for an understanding of the electronic structure of materials. The spectra in the present study recorded below 15 eV are shown in Fig. 5. For the sake of clarity, the main valence band (VB) below 7 eV (top panel) and that between 7 and 14 eV (bottom panel) are shown separately. It can be seen that the VB spectra of the catalysts exhibit broad features around 4 eV (top panel) and relatively sharp peaks around 10 eV (bottom panel). To the main VB observed below 7 eV there could be contributions from valence orbitals of all the relevant elements (Cu, Al, Zr and O). However, owing to the highly ionic character of Al³⁺ and Zr⁴⁺, they do not contribute to the VB and their first lowest occupied core levels of Al 2p and Zr 4p appear around 74 and 30 eV, respectively. At the incident X-ray energy (1253.6 eV) employed in the present experiments, the photoionization cross sections of O 2p and Cu 3d are 0.0005 Mb and 0.021 Mb, respectively and this factor influences mainly the spectral intensity.²⁸ The above data clearly suggest that the Cu 3d have larger contributions than O 2p to the VB, and the broad band around 4 eV can therefore be ascribed to the Cu 3d bands.²⁹ This observation is in good agreement with the XPS-VB of CuO and CuO_x cluster calculations.³⁰ It should be noted that in the present catalyst systems the highest occupied band (below 5 eV) is mainly of Cu 3d character and hence the physicochemical properties of these materials depend on the chemical states of the copper species. It is interesting to note that similar to Cu 2p core levels, the BE of Cu 3d bands for set 1 catalysts (CZAZOC-1, CZAZOC-4 and CZAZOC-6) is higher (4.4 ± 0.1 eV) than that of set 2 catalysts (around 3.7 eV).

The Zn 3d VB appears around 10 eV (see bottom panel of Fig. 5) and this is in agreement with the VB spectrum of ZnO.³¹ The BE of Zn 3d bands, however, varies only marginally (10.0 ± 0.2 eV) and the observed shift is less significant. These results are in line with those observed in the core level XP spectra and suggest a significant modification in the electronic structure of copper species at the catalyst surface with respect to the chemical composition.

Another interesting observation in the VB spectra of these catalysts is the appearance of a shoulder around 2.3 eV in CZAZOC-7. A similar shoulder, albeit with low intensity, can be noticed in CZAZOC-5 and CZAZOC-6 as well. On the other hand, it is very weak or absent in CZAZOC-1 and CZAZOC-4, containing a large amount of Al. This shoulder appears apparently to be due to Cu 3d splitting of the main VB feature around 3.7 eV and can be assigned to the anti-bonding orbitals of the Cu 3d level.^{29–31} This is further supported by the electron-rich environment of set 2 catalysts that

also leads to d orbital splitting. A similar shoulder at 2.3 eV has also been noticed for pure CuO.³⁰ The VB XPS results support the core level XPS results on the existence of a large CuO character on the surface of set 2 catalysts.

In order to get an insight into the surface composition of the catalysts, it has been calculated from the XPS data, taking into account the photoionization cross section, and the results are compared with that of the bulk obtained by XRF chemical analysis of the catalyst precursors (see Fig. 6). A comparison of bulk and surface Cu/Zn ratios (top panel) shows that, in all cases, there is a substantial segregation of Zn at the surface. The Zn enrichment is a maximum in both CZAZOC-5 and CZAZOC-7 (set 2 catalysts) compared to set 1 catalysts. A comparison of the surface Cu/(Al + Zr) atomic ratio with that of the bulk (lower panel), indicates that the surface Cu/(Al + Zr) atomic ratio is close to that of the bulk in the set 1 catalysts while it is higher than that of the bulk in the set 2 catalysts. The surface Cu/(Al + Zr) ratio is very high for CZAZOC-5 probably because of its higher Cu/(Al + Zr) bulk concentration compared to other catalysts (see Table 1).

**Fig. 5** Valence band X-ray photoelectron spectra of CuO/ZnO/Al₂O₃/ZrO₂ mixed oxide catalysts (a) CZAZOC-1, (b) CZAZOC-4, (c) CZAZOC-5, (d) CZAZOC-6 and (e) CZAZOC-7. Top and bottom panels show the main valence band and Zn 3d features, respectively.

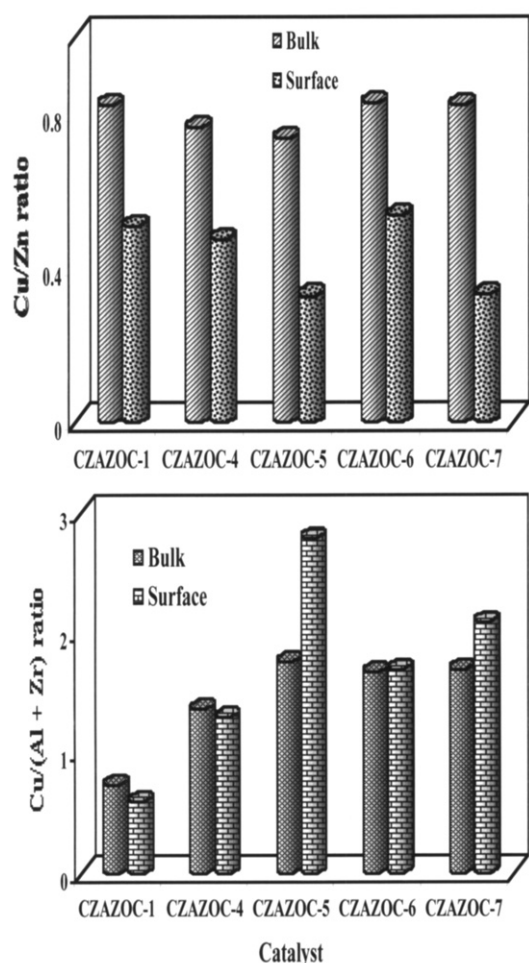


Fig. 6 Comparison of surface Cu/Zn atomic ratio (top panel) and Cu/(Al + Zr) (bottom panel) determined by X-ray photoelectron spectroscopy data with those in the bulk estimated by X-ray fluorescence spectroscopy.

3.3 X-ray absorption spectroscopy

The local structure and electronic states of copper and zinc in these catalysts were investigated by XANES and EXAFS measurements in the Cu K-edge and Zn K-edge regions. The measurements were however limited to three representative samples, namely CZAZOC-4 containing Al without Zr, CZAZOC-6 containing both Al and Zr and CZAZOC-7 containing Zr without Al. The Cu K-edge XANES spectra of the catalysts and those of the reference samples are depicted in Fig. 7 (top panel). The XANES spectrum of Cu foil exhibits the edge absorption (the first inflexion point) at 8979 eV together with a well-resolved doublet in the post-edge region. In the case of CuO, wherein Cu^{2+} exists in a distorted octahedral coordination, the edge transition is observed around 8984 eV. These values for Cu foil and the CuO reference in the present study are in good agreement with those reported in the literature.^{17,20,32} The CuO/ZnO/Al₂O₃/ZrO₂ mixed oxide catalysts also exhibit XANES spectra similar to that of CuO. However, the slope of the edge absorption around 8984 eV is relatively less and it increases with decreasing Al content. The low slope of the edge absorption leads to a shift in the inflexion point of CZAZOC-4 and CZAZOC-6 with respect to the CuO reference. It should be noted, however, that a feature in the pre-edge region around 8978 eV, which is observed in some of the Cu–ZnO and Cu supported on ZrO₂ or Al₂O₃ catalysts,^{30–35} is not visible or is very weak in the present system.

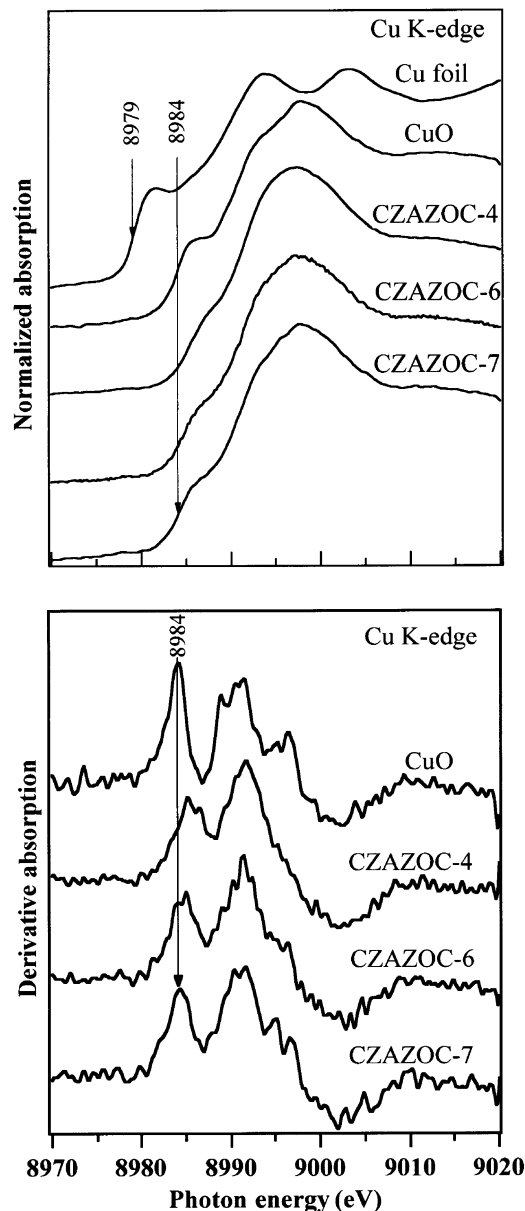


Fig. 7 Cu K-edge XANES spectra of CuO/ZnO/Al₂O₃/ZrO₂ mixed oxide catalysts (top panel). The XANES spectra of Cu foil and CuO references are included for comparison. The bottom panel shows the derivative XANES spectra.

The derivative XANES spectra shown in the bottom panel of Fig. 7 indicate that the edge absorption for CZAZOC-7 coincides very well with that of the CuO reference while a shift can be noticed for other samples. In addition, the shape of the peak above 8990 eV differs considerably for other samples. These results indicate that the chemical environment of copper species in CZAZOC-7 is close to that of the CuO reference while it is different for other samples.

Fig. 8 shows the Zn K-edge XANES spectra of the catalysts. In all cases, the edge absorption is noticed at 9664 eV, caused by the excitation of Zn 1s electrons. Post-edge peaks appear around 9671 and 9681 eV. The edge absorption energy recorded in the present study is a characteristic of Zn²⁺ and is very similar to that reported in the literature for pure ZnO.³⁶ As noticed in the Cu K-edge XANES spectra, the sharpness of the peaks around 9671 and 9681 eV increases with decreasing Al content, and the XANES spectrum of CZAZOC-7 closely resembles that of the pure ZnO reference. How-

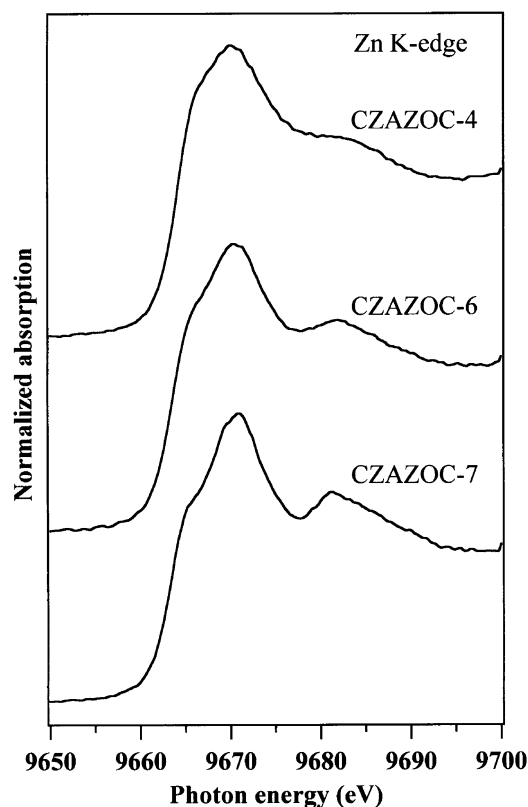


Fig. 8 Zn K-edge XANES spectra of CuO/ZnO/Al₂O₃/ZrO₂ mixed oxide catalysts.

ever, there is no significant change in the slope of the edge absorption and its inflexion point (9664 eV) is identical for all the samples.

The EXAFS measurements in the Cu K-edge region were performed in order to understand the local structure and electronic states of copper in these catalysts. Unfortunately, our attempt to perform EXAFS in the Zn K-edge region was unsuccessful due to the presence of a lot of noise in the spectra. Hence, interpretations in the present study are based only on the results obtained from Cu K-edge EXAFS.

The background subtracted k^3 -weighted EXAFS oscillations, $k^3\chi(k)$, for the catalysts together with that of the CuO reference are presented in Fig. 9. These $k^3\chi(k)$ oscillations were Fourier transformed as shown in Fig. 10. All the samples, including CuO, exhibit two strong peaks, one around 1.45 Å and the other around 2.55 Å due to the Cu–O and Cu–Cu scattering, respectively. The peaks observed in the Fourier transforms of the catalyst samples match very well with those of the CuO.

Since the peaks in the Fourier transformed $k^3\chi(k)$ EXAFS oscillation were well separated, it was possible to obtain the inverse transforms of the individual peaks and hence curve-fitting analysis was performed. A good fit to the inverse transforms of the peaks was obtained using scattering parameters of Cu–O to the first peak (around 1.45 Å) and that of Cu–Cu to the second peak (around 2.55 Å) as illustrated in Fig. 11A and B, respectively. The structural parameters derived from the fitting of the EXAFS oscillations for reference samples and for the catalysts are gathered in Table 4. It can be seen that the Cu–O distance decreases from 1.92 Å for CZA-ZOC-4 to 1.78 Å for CZA-ZOC-7 while the Cu–Cu distance remains around 2.85 Å and is not affected significantly. Another interesting observation noticed in the Fourier transform of the $k^3\chi(k)$ of these samples is the development of a third intense peak around 3.7 Å, which can be clearly observed in the case of CZA-ZOC-7 (see Fig. 10). This peak is absent in CZA-

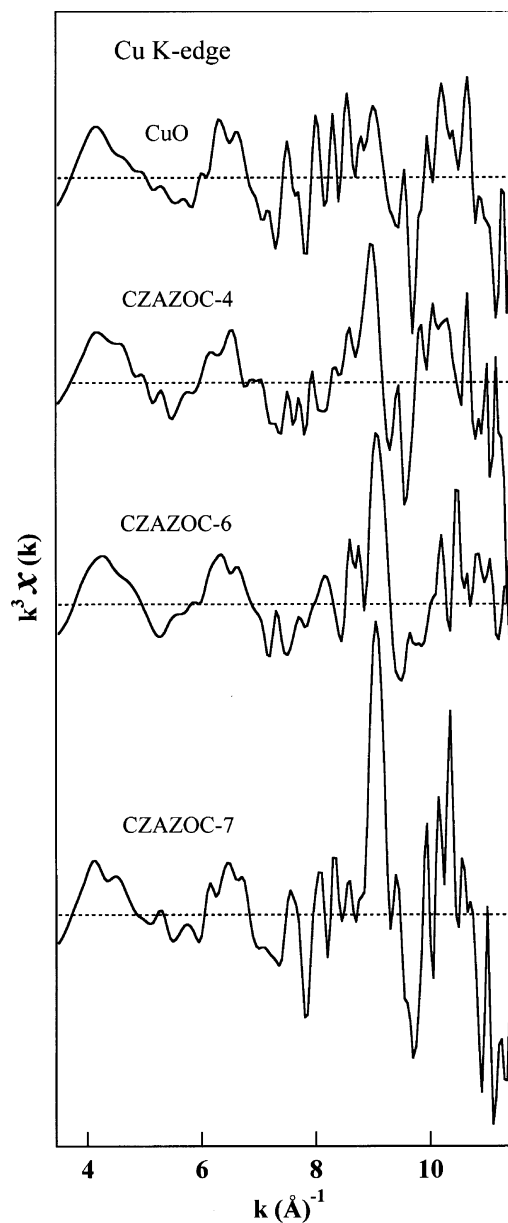


Fig. 9 k^3 -weighted EXAFS oscillations for CuO/ZnO/Al₂O₃/ZrO₂ mixed oxide catalysts. The EXAFS oscillations of CuO reference are included for comparison.

ZOC-4 containing Al without Zr and, it is weak in CZA-ZOC-6 containing both Al and Zr. The inverse transforms of this peak fit fairly well assuming scattering parameters of Cu–Zr bonding (see Fig. 11C). The curve fitting analysis yielded a Cu–Zr distance of 3.87 Å in the case of CZA-ZOC-7 (Table 4). The existence of Cu–Zr scattering has been further substantiated by a nice fitting to the inverse Fourier transformed EXAFS over the whole range ($R = 1.0$ to 4.0 Å) using scattering parameters of Cu–O, Cu–Cu and Cu–Zr together (see Fig. 11D). Fitting was not satisfactory when the scattering parameters of the third shell were other than Cu–Zr thus confirming the existence of a “Cu–O–Zr” bond in the Zr-containing catalysts.

4 Discussion

4.1 XPS studies and the nature of the Cu species

The higher BE of set 1 catalysts comprising CZA-ZOC-1, CZA-ZOC-4 and CZA-ZOC-6 compared to set 2, which includes

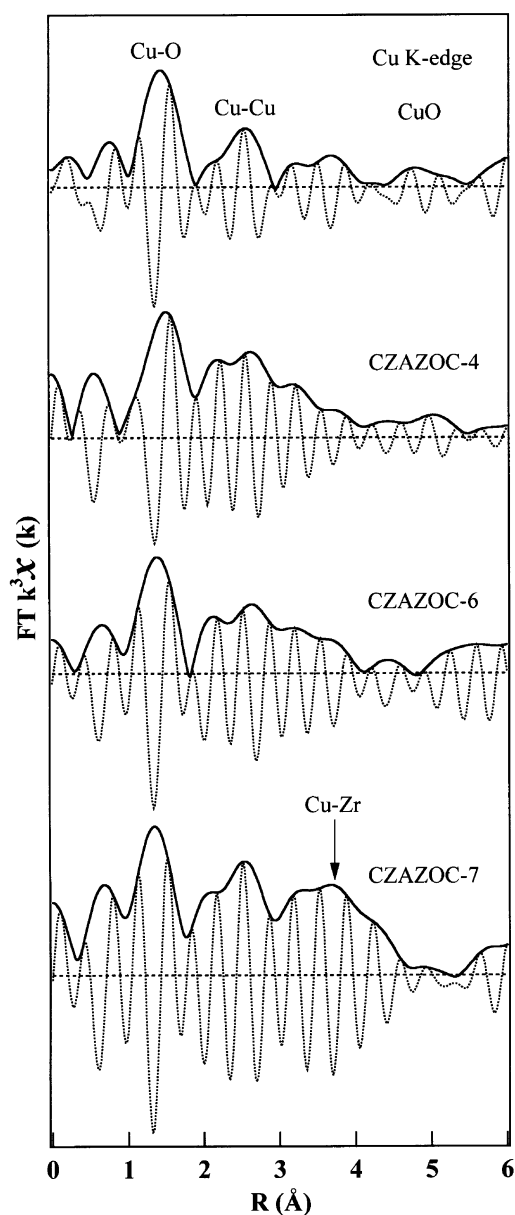


Fig. 10 Non-phase shift corrected Fourier transforms of $k^3\chi(k)$ for CuO/ZnO/Al₂O₃/ZrO₂ mixed oxide catalysts.

CZAZOC-5 and CZAZOC-7 (Fig. 1, Table 2), clearly indicates that the electron density on Cu²⁺ is higher in the set 2 catalysts. The AES results (Fig. 2) corroborate the core level XPS results by exhibiting a similar trend in the KE of the Auger electron as well as the modified Auger parameter α' . Based on the results derived from the Wagner plot and XPS data, the nature of the copper species present in the set 2 catalysts is similar to that in crystalline CuO with more covalent chemical bonding.²⁵ On the other hand, a poorly crystallized CuO having a higher ionicity of chemical bond is present in set 1 catalysts. The formation of surface CuAl₂O₄ spinel was often noticed when Al was present in the sample.⁴ In XPS, the CuAl₂O₄ surface spinel species are characterized by a higher Cu 2p_{3/2} BE (by *ca.* 1 eV) and a lower Auger KE of Cu LMM compared to that of CuO. Thus, the higher BE and lower Auger KE in the core level XPS of set 1 catalysts could be due to the formation of surface CuAl₂O₄ species, and this is in agreement with the results derived from UV-Vis DRS, EPR and TPR.¹² The higher BE of the main VB for set 1 catalysts also supports this conclusion.

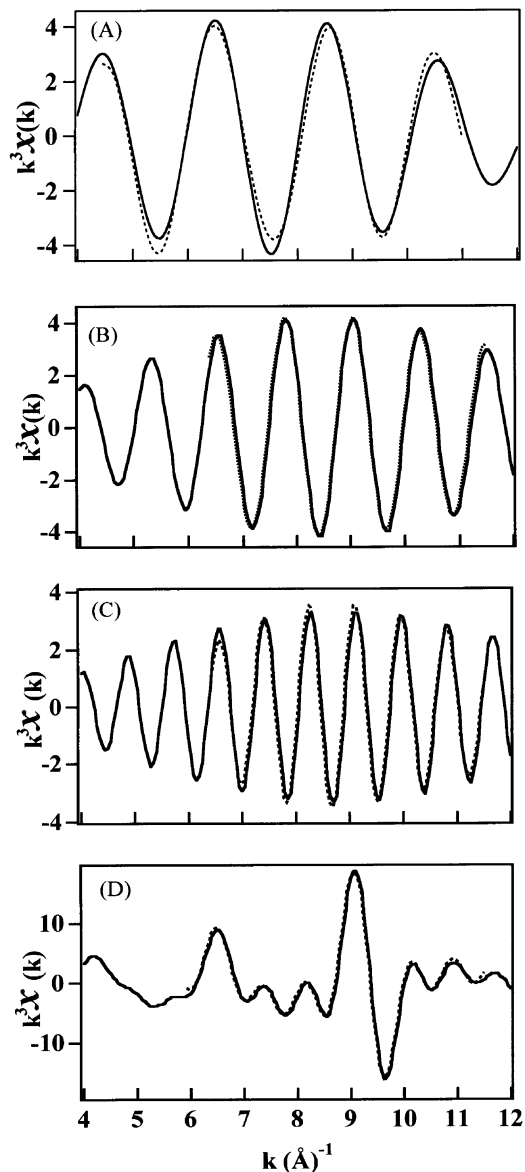


Fig. 11 Examples for the best fitting of Fourier back-filtered EXAFS oscillations. The fittings of first shell, second shell and third shell of CZAZOC-7 are shown. (A) First shell (Cu–O scattering), (B) second shell (Cu–Cu scattering), (C) third shell (Cu–Zr scattering), (D) curve fitting of the inverse Fourier transform EXAFS over the whole range ($R = 1.0$ to 4.0 Å) using scattering parameters of CuO, CuCu and Cu–Zr together. Solid curves: inverse transform, dotted curves: calculated EXAFS.

The I_S/I_M ratio of between 0.40 and 0.46 and the FWHM of Cu 2p_{3/2} (3.4 ± 0.1 eV) observed in both set 1 and set 2 catalysts (Table 2) are less than those observed for pure CuO ($I_S/I_M = 0.55$ and FWHM = 3.6 eV).¹ A decrease in the I_S/I_M ratio has been previously observed upon addition of ZnO, particularly for materials with low Cu/Zn ratios.³⁷ The result has been attributed to the dissolution of Cu²⁺ species in ZnO. Moretti *et al.*,¹ on the other hand, attributed this phenomenon to the existence of a strong interaction between CuO and ZnO and leading to a more covalent Cu–O bond, and as a consequence the I_S/I_M ratio decreased. The observation, that the catalyst surface is enriched with Zn (see Fig. 6) and that the BE of the Zn 2p_{3/2} core level and its FWHM are not affected by the change in the chemical composition, clearly indicate that the CuO-like species are surrounded by ZnO. There is no evidence of Cu dissolution in ZnO or Zn dissolution in CuO in the present catalytic system, in contrast to that

Table 4 Structural parameters of CuO/ZnO/Al₂O₃/ZrO₂ mixed oxide catalysts fitted to EXAFS oscillations^a

Sample	Atom pair	<i>N</i>	<i>R</i> /Å	$\Delta\sigma^2/10^{-3}\text{\AA}^2$
Cu foil	Cu–Cu	4.9	2.55	5.9
CuO	Cu–O	1.0	1.88	5.3
	Cu–Cu	2.1	2.88	2.4
CZAZOC-4	Cu–O	0.6	1.92	0.9
	Cu–Cu	2.1	2.85	2.8
CZAZOC-6	Cu–O	0.5	1.83	2.7
	Cu–Cu	2.2	2.90	2.8
	Cu–Zr	0.6	3.46	5.8
CZAZOC-7	Cu–O	1.1	1.78	3.0
	Cu–Cu	1.9	2.85	1.1
	Cu–Zr	3.0	3.87	7.4

^a Fitting range (Δk) = 5–10 Å⁻¹ for Cu–O, and 6.5–11.5 Å⁻¹ for Cu–Cu/Zn/Zr. Reference data: ¹⁶Cu–Cu bond distance in Cu metal = 2.56 Å; Cu–Cu and Cu–O bond distances in CuO = 2.90 and 1.95 Å, respectively.

reported by a few researchers for the methanol synthesis CuO/ZnO system.^{16,37}

The Zr 3d XPS of Zr-containing catalysts (Fig. 4) clearly show the presence of zirconium sites (species I) with relatively higher electron density. The relative concentration of species I is higher than that of species II (see Table 3) in CZAZOC-7 containing a higher Zr content. The increase in the concentration of Zr species I with increasing Zr content reveals the existence of a Cu–Zr synergistic interaction in the Zr-containing samples and this is further substantiated from the VB XPS. The low BE of the main VB involving Cu 3d valence electrons in CZAZOC-5 and CZAZOC-7 and the splitting of the Cu 3d anti-bonding levels from the main VB (Fig. 5) clearly imply that the Cu 3d antibonding orbitals are significantly populated in these catalysts. The relatively higher intensity of the shoulder at 2.3 eV corresponding to the Cu 3d anti-bonding orbitals in CZAZOC-7 suggests that the splitting of the main VB is more pronounced in this catalyst. Thus, the higher concentration of Zr species I and the higher intensity of the Cu 3d anti-bonding orbital in CZAZOC-7 containing more zirconium strongly suggests the existence of a Cu–Zr synergistic interaction and the Cu–Zr interacting species is dominating at the surface of CZAZOC-7. The existence of such a Cu–Zr synergistic interaction could be responsible for the improved reducibility of Cu²⁺ in the CZAZOC-7 catalyst as observed by the TPR experiments.¹²

4.2 XANES and EXAFS studies

The XANES spectra are associated with the excitation of a core electron to bound and quasi-bound states. To determine the valence and coordination geometry of copper in these catalysts, the Cu K-edge XANES was compared with that of Cu foil and CuO standards for which the oxidation states and site distributions of copper are known. In general, the position and shape of different features in the near-edge structure are essentially influenced by the effective charge of the absorbing species, the coordination geometry and the formal charge. An intense edge absorption at 8984 eV observed for CuO (Fig. 7) has been assigned to the 1s → 4p transition of octahedral or tetragonally distorted octahedral symmetry of Cu²⁺.³⁸ The low slope of the edge absorption for CZAZOC-4 and CZAZOC-6 compared to that of CZAZOC-7 could be due to the low intensity of the peak around the edge (*ca.* 8985.5 eV) and this suggest some changes in the chemical environment around the Cu²⁺ species in those samples. Similar results were also observed in the XANES spectra of Cu in ZnO methanol synthesis catalysts and attributed to a further distortion of

Cu²⁺ sites to a tetrahedral geometry due to the dissolution of a part of the Cu in the ZnO lattice, thereby generating a solid solution.³² However, in the above investigations, the authors also observed a weak pre-edge peak at 8978 eV due to the 1s → 3d transition, which in the case of an octahedral geometry is dipole-forbidden and quadrupole-allowed. The intensity of this pre-edge peak in the above Cu/ZnO samples increased as the distortion of the Cu²⁺ environment increased. Such a weak pre-edge peak was however not observed in the present catalysts. The absence of the pre-edge peak in these catalysts clearly indicates the existence of Cu²⁺ in a regular octahedral coordination without much distortion. These results further substantiate the XPS results on the non-formation of Cu-doped ZnO solid solution in the present catalyst systems. The XANES results however indicate that the chemical environment of copper species in set 2 catalysts, particularly in CZAZOC-7, is close to that of the CuO reference while it is different for other samples.

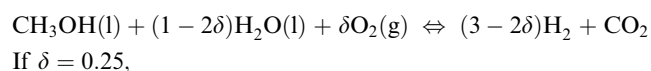
The position of the edge absorption in Zn K-edge (Fig. 8) remains almost identical for all the samples, indicating that the chemical environment around Zn²⁺ is not influenced by the chemical composition. This result is in agreement with the Zn 2p_{3/2} XPS data. However, the sharpness of the post-edge peaks in both the Cu K-edge and the Zn K-edge increases from CZAZOC-4 to CZAZOC-7 and this might be due to an increase in the crystallinity of the CuO and ZnO phases, as evidenced from a gradual increase in the XRD intensity in the same order.¹²

The EXAFS study indicates that in all cases CuO-like species are present with a Cu–O distance of 1.8 to 1.9 Å and Cu–Cu distance of about 2.9 Å which are very close to those of CuO (Table 4). In the Zr-containing catalysts, in addition to the Cu–O and Cu–Cu atom pairs, the existence of Cu–Zr atom pair with a distance of 3.5 to 3.9 Å is also noticed. This observation suggests the formation of Zr⁴⁺-doped CuO in the Zr-containing catalysts. Although the XRD, XPS and XANES results indicate the presence of a well crystallized CuO phase in Zr-rich CZAZOC-7, the EXAFS display marked differences from such a phase (lower Cu–O distance; see Table 4) suggesting the presence of a Cu–Zr mixed oxide/solid solution with geometrical/electronic differences from CuO. The formation of such a solid solution brings about a synergistic interaction between copper and amorphous zirconia, as evidenced from the XPS data.

Earlier EXAFS studies¹⁶ on the CuO/ZnO methanol synthesis catalysts have identified an additional less intense peak around 3.02 Å. This peak has been attributed to the formation of the Cu–Zn atom pair and the existence of Cu²⁺ in the substitutional sites of ZnO was concluded. The Fourier analysis of the EXAFS corresponding to CuO in our study does not exhibit any peak in this region (Fig. 10). This further substantiates the absence of Cu-containing ZnO or Zn-containing CuO solid solutions in these catalyst systems in agreement with the XPS and XANES data.

4.3 Cu–Zr interaction and catalytic performance

A detailed study of the performance of these catalysts in the OSRM reaction described in eqn. (2) has already been reported.^{12,14}



$$\Delta H^\circ_{298} = -12.0 \text{ kJ mol}^{-1} \text{ and } \Delta G^\circ_{298} = -109.6 \text{ kJ mol}^{-1} \quad (2)$$

Since the reaction was performed after reducing the catalysts *in situ* at 300 °C prior to the reaction, the authors feel that it is more appropriate to correlate the physicochemical properties

of the reduced catalysts rather than the unreduced oxide catalysts with catalytic activity. However, there could be a rough correlation between the Cu–Zr interaction derived from XPS, XANES and EXAFS measurements on the unreduced oxide catalysts and catalytic performance. For instance, the catalyst, CZAZOC-7 was found to be the most active in the OSRM reaction exhibiting a methanol conversion above 90% with a H₂ production rate of about 170 mmol kg(catalyst)⁻¹ s⁻¹ at 230 °C. The catalytic activity was found to improve with increasing Zr content. Thus, the higher catalytic activity of CZAZOC-7 could be due to the existence of a strong synergistic interaction between copper and amorphous zirconia species, as evidenced from XPS and XAS (XANES and EXAFS) data. It should be recalled that the XPS indicated the existence of electron-rich zirconium species in the Zr-containing catalysts (Fig. 4, Table 3). Furthermore, the Cu 3d anti-bonding orbitals split from the main VB and appear at lower BE. The formation of Cu–Zr bonding with a distance of 3.5 to 3.9 Å has been confirmed by EXAFS measurements. The existence of such a synergistic interaction, demonstrated clearly in the present study, is likely to improve the copper dispersion, copper metal surface area and copper reducibility, as observed already from our TPR and CO chemisorption experiments,^{12,14} and in consequence lead to an improved catalytic performance. The XPS, XANES and EXAFS results also support the hypothesis of Breen and Ross⁹ and Shu *et al.*⁷ in their investigations on the similar CuO/ZnO/ZrO₂ catalysts for the SRM and methanol synthesis reactions. The addition of ZrO₂ is also reported to adjust the Cu¹⁺/Cu⁰ ratio of the reduced catalyst.⁹ In fact, our *in situ* XRD, XPS and XAS study of the same catalyst after reduction in H₂ showed the existence of Cu¹⁺ and Cu⁰ on the catalyst surface (unpublished results). The correlation between the nature of the active species (Cu¹⁺/Cu⁰) in the reduced catalysts and the catalytic performance in the OSRM reaction is the subject of a further investigation and will be reported separately.

Conclusions

The CuO/ZnO/Al₂O₃/ZrO₂ mixed oxide catalysts employed in the oxidative steam reforming of methanol for H₂ production have been characterized systematically using combined XPS, XANES and EXAFS measurements. The salient findings of the present study are:

(1) The CuO/ZnO/Al₂O₃/ZrO₂ mixed oxide catalysts consist of a CuO solid solution (CuO-like species) in which a part of the Zr is dissolved in the Zr-containing samples. The Cu–O and Cu–Cu distances are about 1.90 and 2.90 Å, respectively while the Cu–Zr distance is in the range 3.5 to 3.9 Å. The CuO-like species are homogeneously distributed on the amorphous Al₂O₃ and/or ZrO₂ phases and, the ZnO decorates the CuO-like species at the surface of all catalysts.

(2) In the catalysts with low Al content, the Cu 3d anti-bonding orbitals split from the main VB and shift toward lower BE. This phenomenon is more pronounced in the catalyst containing Zr without Al and accounts for the improved redox properties of the catalyst.

(3) The presence of zirconium in these catalysts brings about a synergistic interaction with copper species and such a Cu–Zr synergistic interaction should be responsible for the improved reducibility and catalytic activity in the oxidative steam reforming of methanol for H₂ production.

Acknowledgement

The authors would like to express their sincere gratitude to the Japan Science and Technology Corporation (JST) for financial

support for S.V through the Cooperative System for Supporting Priority Research.

References

- G. Moretti, G. Fierro, M. L. Jacono and P. Porta, *Surf. Interface Anal.*, 1989, **14**, 325.
- G. Fierro, M. L. Jacono, M. Inversi, P. Porta, F. Cioci and R. Lavecchia, *Appl. Catal. A*, 1996, **137**, 327.
- J. G. Nunan, P. B. Himelfarb, R. G. Herman, K. Klier, C. E. Bogdan and G. W. Simmons, *Inorg. Chem.*, 1989, **28**, 3868.
- F. Severino, J. L. Brito, J. Laine, J. L. G. Fierro and A. L. Agudo, *J. Catal.*, 1998, **177**, 82.
- Y. Ma, Q. Sun, D. Wu, W. Fan, Y. Zhang and J. Deng, *Appl. Catal. A*, 1998, **171**, 45.
- J. Wu and M. Saito, *J. Catal.*, 2000, **195**, 420.
- Y.-W. Suh, S.-H. Moon and H.-K. Rhee, *Catal. Today*, 2000, **63**, 447.
- J. P. Breen, F. C. Meunier and J. R. H. Ross, *Chem. Commun.*, 1999, 2247.
- J. P. Breen and J. R. H. Ross, *Catal. Today*, 1999, **51**, 521.
- L. Alejo, R. Lago, M. A. Peña and J. L. G. Fierro, *Appl. Catal. A*, 1997, **162**, 281.
- S. Velu, K. Suzuki and T. Osaki, *Chem. Commun.*, 1999, 2341.
- S. Velu, K. Suzuki, M. Okazaki, M. P. Kapoor, T. Osaki and F. Ohashi, *J. Catal.*, 2000, **194**, 373.
- S. Velu, K. Suzuki and T. Osaki, *Catal. Lett.*, 2000, **69**, 43.
- S. Velu, K. Suzuki, M. P. Kapoor, F. Ohashi and T. Osaki, *Appl. Catal. A*, 2001, **213**, 47.
- K. Jung and A. T. Bell, *J. Catal.*, 2000, **193**, 207.
- G. Sankar, S. Vasudevan and C. N. R. Rao, *J. Chem. Phys.*, 1986, **85**, 2291.
- I. J. Shannon, F. Rey, G. Sanker, J. M. Thomas, T. Maschmeyer, A. W. Waller, A. E. Palomares, A. Corma, A. J. Dent and G. N. Greaves, *J. Chem. Soc., Faraday Trans.*, 1996, **92**, 4331.
- T. L. Reitz, P. L. Lee, K. F. Czaplewski, J. C. Lang, K. E. Popp and H. H. Kung, *J. Catal.*, 2001, **199**, 193.
- Y. Udagawa, in *X-ray Absorption Fine Structure for Catalysts and Surfaces*, ed. Y. Iwasawa, World Scientific, Singapore, 1996, p. 140.
- T. Yoshida, T. Tanaka, H. Yoshida, T. Funabiki and S. Yoshida, *J. Phys. Chem.*, 1996, **100**, 2302.
- K. Nishi, K. Shimizu, M. Takamatsu, H. Yoshida, A. Satsuma, T. Tanaka, S. Yoshida and T. Hattori, *J. Phys. Chem. B*, 1998, **102**, 10190.
- J. J. Rehr, L. de Mustre, S. I. Zabinsky and R. C. Albers, *J. Am. Chem. Soc.*, 1991, **113**, 5135.
- I. Grohmann, B. Peplinski and W. Unger, *Surf. Interface Anal.*, 1992, **19**, 591.
- P. Porta, M. C. Campa, G. Fierro, M. L. Jacono, G. Minelli, G. Moretti and L. Stoppa, *J. Mater. Chem.*, 1993, **3**, 505.
- G. Moretti, *J. Electron Spectrosc. Relat. Phenom.*, 1995, **76**, 365.
- S. Poulston, P. M. Parlett, P. Stone and M. Bowker, *Surf. Interface Anal.*, 1996, **24**, 811.
- S. Ardizzone and C. L. Bianchi, *Surf. Interface Anal.*, 2000, **30**, 77.
- J. J. Yeh and I. Lindau, *At. Data Nucl. Data Tables*, 1985, **32**, 1.
- S. V. Didziulis, K. D. Butcher, S. L. Cohen and E. I. Solomon, *J. Am. Chem. Soc.*, 1989, **111**, 7110.
- J. Ghijsen, L. H. Tjeng, J. van Elp, H. Eskes, J. Westerink and G. A. Sawatzky, *Phys. Rev. B*, 1988, **39**, 11322.
- J. Lin, P. Jones, J. Guckert and E. I. Solomon, *J. Am. Chem. Soc.*, 1991, **113**, 8312.
- G. Meitzner and E. Iglesia, *Catal. Today*, 1999, **53**, 433.
- L.-S. Kau, O. H. Hodgson and E. I. Solomon, *J. Am. Chem. Soc.*, 1989, **111**, 7103.
- Y. Okamoto, H. Gotoh, H. Aritani, T. Tanaka and S. Yoshida, *J. Chem. Soc., Faraday Trans.*, 1997, **93**, 3879.
- K. Shimizu, H. Maeshima, H. Yoshida, A. Satsuma and T. Hattori, *Phys. Chem. Chem. Phys.*, 2000, **2**, 2435.
- J. A. Biscardi, G. D. Meitzner and E. Iglesia, *J. Catal.*, 1998, **179**, 192.
- Y. Okamoto, F. Fukino, K. Imanaka and S. Teranishi, *J. Phys. Chem.*, 1983, **87**, 3740.
- D. DeBeer, D. W. Randall, A. M. Nersissian, J. S. Valentine, B. Hedman, K. O. Hodgson and E. I. Solomon, *J. Phys. Chem. B*, 2000, **104**, 10814.